Discontinuous molecular dynamics for rigid bodies: Applications

Lisandro Hernández de la Peña, Ramses van Zon, and Jeremy Schofield
Chemical Physics Theory Group, Department of Chemistry, University of Toronto, Ontario M5S 3H6, Canada

Sheldon B. Opps
Department of Physics, University of Prince Edward Island, 550 University Avenue, Charlottetown, Prince Edwards Island C1A 4P3, Canada

(Received 20 July 2006; accepted 28 December 2006; published online 20 February 2007)

Event-driven molecular dynamics simulations are carried out on two rigid-body systems which differ in the symmetry of their molecular mass distributions. First, simulations of methane in which the molecules interact via discontinuous potentials are compared with simulations in which the molecules interact through standard continuous Lennard-Jones potentials. It is shown that under similar conditions of temperature and pressure, the rigid discontinuous molecular dynamics method reproduces the essential dynamical and structural features found in continuous-potential simulations at both gas and liquid densities. Moreover, the discontinuous molecular dynamics approach is demonstrated to be between 3 and 100 times more efficient than the standard molecular dynamics method depending on the specific conditions of the simulation. The rigid discontinuous molecular dynamics method is also applied to a discontinuous-potential model of a liquid composed of rigid benzene molecules, and equilibrium and dynamical properties are shown to be in qualitative agreement with more detailed continuous-potential models of benzene. The few qualitative differences in the angular dynamics of the two models are related to the relatively crude treatment of variations in the discontinuous repulsive interactions as one benzene molecule rotates by another. © *2007 American Institute of Physics*. [DOI: 10.1063/1.2434959]

I. INTRODUCTION

Although event-driven simulation studies of systems of molecules interacting via discontinuous potentials are common,[1–5] most work to date has considered models in which constituent atoms of a molecule represented as point particles interact through pairwise, stepped, discontinuous potentials.[6] Event-driven simulations of these kinds of models have been successfully used to study conformational transitions in biomolecular systems.[6–8] However, in the atom or point-particle based simulations, a great deal of computational effort is devoted to treating essentially unimportant internal motion of molecules. This is true both for event-driven simulations, whose efficiency depends critically on the number of events to process per unit of simulation time, and for standard continuous-potential models of molecular systems. To extend the time scale or system size accessible to simulations, the molecules can be modeled as rigid bodies, although this requires additional techniques.

For standard molecular dynamics of molecules interacting via continuous potentials, techniques to perform efficient simulations of rigid systems were developed some time ago. In the preceding paper,[10] a general framework to carry out event-driven simulations of molecular systems interacting via discontinuous potentials in the presence of constraints was outlined. This formalism is generally applicable to both semiflexible and fully rigid bodies. In the case of a rigid molecular system, it was shown that the analytical solution of the free motion of arbitrary rigid bodies can be combined with efficient numerical algorithms for the search for event times and the use of appropriate collision rules to carry out event-driven or discontinuous molecular dynamics (DMD) simulations.

In the present work, we apply this approach to two molecular systems of practical interest, methane and benzene. The lack of similarity in the mass distribution of methane and benzene molecules, classified as spherical and symmetric top rotors, respectively, implies that the rotational motion in these two systems is quite different. First, a discontinuous-potential model of rigid molecular methane is constructed by analogy with a standard continuous-potential model based on Lennard-Jones interactions. Structural and dynamical characteristics of DMD simulations obtained at gas and liquidlike densities are then compared to their analogs in the continuous-potential system, and the computational efficiency of the DMD approach is contrasted with standard molecular dynamics (SMD) simulations. Second, a discontinuous model of a liquid of rigid molecules of benzene is designed to compare to a united-atom model of rigid molecules interacting with continuous potentials. Equilibrium and dynamical properties of both models are compared under similar conditions of density and temperature. The dynamics of orientational degrees of freedom is examined and the few discrepancies observed in details of the angular motion are explained.

The paper is organized as follows. The methane system is studied in Sec. II, starting with a discussion of general considerations pertinent for performing DMD as well as continuous-potential simulations of a symmetric-top, rigid molecular system in part A, followed by the presentation of

 © 2007 American Institute of Physics

Downloaded 14 May 2007 to 142.150.224.6. Redistribution subject to AIP license or copyright, see http://jcp.aip.org/jcp/copyright.jsp

gas phase results, the liquid phase simulation results, and analysis of computational efficiency in parts B, C, and D, respectively. In Sec. III, simulations of a united-atom model of rigid benzene are presented. Continuous and discontinuous-potential models are presented in part A, followed by a discussion of the simulation details and the equilibrium properties results in parts B and C, respectively. A detailed analysis of the dynamical results, including a careful examination of the discrepancies associated with the differences between the models, is provided in part D of this section. Finally, conclusions are discussed in Sec. IV.

II. RIGID METHANE

A. Specification of the model

Consider a system of rigid methane molecules in which the four hydrogen atoms are held fixed with bond length d in a tetrahedral arrangement around the central carbon atom. If the mass of the hydrogen atoms is taken to be the mass of one proton m_p, and the mass of the central carbon is $12m_p$, the principal moments of inertia of the rigid rotor system are all equal and given by $I_1=I_2=I_3=8m_pd^2/3$.

For this rigid molecular model of methane, discontinuous interaction potentials can be constructed by combining repulsive hard-core and attractive square-well interactions as follows: The repulsive hard-core interaction potential between site i on molecule a and site j on molecule b is given by

$$V_{ij}^{\mathrm{rep}}(r_{ij}^{ab})=\begin{cases}\infty & \text{if } r_{ij}^{ab}\leqslant d_{ij}\\ 0 & \text{if } r_{ij}^{ab}>d_{ij},\end{cases} \tag{1}$$

where $r_{ij}^{ab}=|\boldsymbol{r}_i^a-\boldsymbol{r}_j^b|$ denotes the distance between site i of molecule a and site j of molecule b, and d_{ij} is the interaction distance. In the model for methane, we assume that all hydrogen atoms on different molecules interact via a hard-core repulsive interaction at a distance d_{HH}, while carbon atoms and carbon-hydrogen atoms on different molecules repel at d_{CC} and d_{CH}, respectively.

In addition to the hard-core repulsive interaction potentials above, we include an attractive square well (SW) between carbon atoms in the model of the form

$$V_{\mathrm{CC}}^{\mathrm{attr}}(r_{\mathrm{CC}}^{ab})=\begin{cases}-V_{\mathrm{SW}} & \text{if } r_{\mathrm{CC}}^{ab}\leqslant d_{\mathrm{SW}}\\ 0 & \text{if } r_{\mathrm{CC}}^{ab}>d_{\mathrm{SW}},\end{cases} \tag{2}$$

where the values of V_{SW} and d_{SW} are adjustable parameters and the obvious condition $d_{\mathrm{SW}}>d_{\mathrm{CC}}$ must hold for this potential to have any effect. The attractive potential allows for a condensation transition in a dense fluid of methane molecules at low temperature.

Given the form of the potentials in the model, the *exact* trajectory can be computed from arbitrary initial conditions.[11] At any time t, the orientation of a given methane molecule is specified by a rotation matrix $\mathbf{A}(t)$, known as the *attitude matrix*, while its center of mass undergoes a free linear motion in between impulsive events. The attitude matrix and its transpose $\mathbf{A}^{\dagger}(t)$ can be used to transform between the laboratory and principal axis (body) frames and to calculate the Cartesian positions $\boldsymbol{r}_i(t)$ of an atom i in a molecule using

$$\boldsymbol{r}_i(t)=\boldsymbol{R}(t)+\mathbf{A}^{\dagger}(t)\cdot\tilde{\boldsymbol{r}}_i=\boldsymbol{R}(0)+\boldsymbol{V}(0)t+\mathbf{A}^{\dagger}(t)\cdot\tilde{\boldsymbol{r}}_i, \tag{3}$$

where $\tilde{\boldsymbol{r}}_i$ is the constant position vector in the body frame, and $\boldsymbol{R}$ and $\boldsymbol{V}$ are the Cartesian vectors in the laboratory frame for the center-of-mass position and velocity, respectively.

As discussed in detail in Ref. 10, the time dependence of the attitude matrix is given by

$$\mathbf{A}(t)=\mathbf{P}(t)\mathbf{A}(0), \tag{4}$$

where $\mathbf{P}(t)$ is a rotation matrix itself which "propagates" the orientation $\mathbf{A}(0)$ to the orientation at time t. For a spherical rotor, such as methane, in which all the principal moments of inertia are equal, the propagator matrix $\mathbf{P}(t)$ is particularly simple,

$$\mathbf{P}(t)=\mathbf{U}(-\tilde{\boldsymbol{\omega}}t), \tag{5}$$

where $\tilde{\boldsymbol{\omega}}$ is the angular velocity vector in the body frame. In Eq. (5), $\mathbf{U}(-\tilde{\boldsymbol{\omega}}t)=\mathbf{U}(\theta\hat{\boldsymbol{n}})$ is a rotation matrix rotating an arbitrary vector by an angle $\theta=-|\tilde{\boldsymbol{\omega}}|t$ around an axis $\hat{\boldsymbol{n}}=\tilde{\boldsymbol{\omega}}/|\tilde{\boldsymbol{\omega}}|$ with components (n_1,n_2,n_3) according to

$$\mathbf{U}(\theta\hat{\boldsymbol{n}})=\mathbf{I}+\mathbf{W}(\hat{\boldsymbol{n}})\sin\theta+\mathbf{W}(\hat{\boldsymbol{n}})\mathbf{W}(\hat{\boldsymbol{n}})(1-\cos\theta), \tag{6}$$

where $\mathbf{I}$ is the identity matrix and $\mathbf{W}$ is the skew-symmetric matrix

$$\mathbf{W}(\hat{\boldsymbol{n}})=\begin{pmatrix}0 & -n_3 & n_2\\ n_3 & 0 & -n_1\\ -n_2 & n_1 & 0\end{pmatrix}. \tag{7}$$

For a spherical rotor, it follows from the Euler equations that $\tilde{\boldsymbol{\omega}}$ is a constant vector determined by initial conditions, and hence the matrix $\boldsymbol{U}(-\tilde{\boldsymbol{\omega}}t)$ can be viewed as a rotation around a fixed axis by an angle that is a linear function of time. Note that the moments of inertia tensor in the laboratory frame $\mathbf{I}(t)$ and in the principal axis frame $\tilde{\mathbf{I}}$ are related by $\mathbf{I}(t)=\mathbf{A}^{\dagger}(t)\cdot\tilde{\mathbf{I}}\cdot\mathbf{A}(t)$, with $\tilde{\mathbf{I}}=\mathrm{diag}(I_1,I_1,I_1)$ for a spherical rotor, implying that $\mathbf{I}(t)$ is diagonal, constant, and equal to the moment of inertia tensor in the principal axis frame $\tilde{\mathbf{I}}$.

The angular momentum vector $\tilde{\boldsymbol{\omega}}$, defining the axis of rotation in $\mathbf{P}(t)$, remains constant until an impulsive force acts on it during a collision event. The times t_c at which the impulses act are determined by zeros of a collision indicator function $f_{ij}(t_c)=[r_{ij}^{ab}(t_c)]^2/2-d_{ij}^2/2$, describing the time $t=t_c$ at which the distance $r_{ij}^{ab}(t)$ between atom i of body a and atom j of body b attains a value at which there is a discontinuity in the potential energy [see Eq. (1)]. As explained in Ref. 10, the collision times can be computed using numerical grid-search methods using Eq. (3).

The effect of the impulses on the Cartesian coordinates or angular velocities can be computed either from a constrained variable approach or using a rigid-body approach.[10] In the rigid-body approach, the impulse at collision time t_c leads to a discontinuity in the center-of-mass momentum vector $\boldsymbol{P}_a$ and angular velocity vector $\boldsymbol{\omega}_a$ of body a in the laboratory frame according to

$$\boldsymbol{P}_a'=\boldsymbol{P}_a+\Delta\boldsymbol{P}_a, \tag{8}$$

Downloaded 14 May 2007 to 142.150.224.6. Redistribution subject to AIP license or copyright, see http://jcp.aip.org/jcp/copyright.jsp

$$\boldsymbol{\omega}_a' = \boldsymbol{\omega}_a + \Delta\boldsymbol{\omega}_a, \tag{9}$$

where $\boldsymbol{P}_a = M\boldsymbol{V}_a$ is the center-of-mass momentum vector of body a, M is the total mass of body a, and $\boldsymbol{P}_a'$ and $\boldsymbol{\omega}_a'$ indicate the postcollisional center-of-mass momentum and angular velocity vectors. Application of conservation laws leads to the following results:

$$\Delta\boldsymbol{P}_a = -S\hat{\boldsymbol{r}}_{ij}^{ab}, \tag{10}$$

$$\Delta\boldsymbol{\omega}_a = -S\mathbf{I}_a^{-1}(\bar{\boldsymbol{r}}_i^a \times \hat{\boldsymbol{r}}_{ij}^{ab}), \tag{11}$$

where S is the magnitude of the impulse given by

$$S = \frac{-b \pm \sqrt{b^2 - 4a\Delta\Phi}}{2a}, \tag{12}$$

where $\Delta\Phi$ is the height of the discontinuity in the potential at the interaction distance, and

$$2a = \frac{1}{M_a} + \frac{1}{M_b} + \boldsymbol{n}_{ij}^a \cdot \mathbf{I}_a^{-1}\boldsymbol{n}_{ij}^a + \boldsymbol{n}_{ij}^b \cdot \mathbf{I}_b^{-1}\boldsymbol{n}_{ij}^b$$

$$b = \boldsymbol{v}_{ij}^{ab} \cdot \hat{\boldsymbol{r}}_{ij}^{ab},$$

with $\boldsymbol{n}_{ij}^a = \bar{\boldsymbol{r}}_i^a \times \hat{\boldsymbol{r}}_{ij}^{ab}$ and $\boldsymbol{n}_{ij}^b = \bar{\boldsymbol{r}}_j^b \times \hat{\boldsymbol{r}}_{ij}^{ab}$. Note that we have dropped the explicit time arguments here. In the equations above, all quantities are to be taken at time $t = t_c$ and $\bar{\boldsymbol{r}}_i^a = \boldsymbol{r}_i^a - \boldsymbol{R}^a$ denotes the position vector of atom i on molecule a relative to its center of mass $\boldsymbol{R}^a$ and $\hat{\boldsymbol{r}}_{ij}^{ab}$ is the unit vector along the direction of the vector $\boldsymbol{r}_j^b - \boldsymbol{r}_i^a$ connecting atom i on body a with its colliding partner j on body b. The relative velocity vector v_{ij}^{ab} at the point of contact can be written in terms of the angular velocities using $\boldsymbol{v}_{ij}^{ab} = \boldsymbol{v}_j^b - \boldsymbol{v}_i^a = \boldsymbol{V}_b - \boldsymbol{V}_a + \boldsymbol{\omega}_b \times \bar{\boldsymbol{r}}_j^b - \boldsymbol{\omega}_a \times \bar{\boldsymbol{r}}_i^a$. The physical solution for S corresponds to the positive (negative) square root if $b > 0$ ($b < 0$), provided $b^2 > 4a\Delta\Phi$. If this latter condition is not met, there is not enough kinetic energy to overcome the discontinuous barrier and the system experiences a hard-core scattering, in which case $\Delta\Phi$ is replaced by zero and consequently $S = -b/a$. For the spherical rotor methane system, the fact that $\tilde{\mathbf{I}} = \mathrm{diag}(I_1, I_1, I_1)$ leads to the simplification $\Delta E_\omega^{a,b} = \boldsymbol{n}_{ij}^{a,b} \cdot \boldsymbol{n}_{ij}^{a,b}/I_1$.

With this model in hand, a DMD simulation can be carried out where four different types of events can take place, namely, hard-core collisions, square-well interactions, cell crossings, and virtual collisions associated with the truncation of numerical searches[14] for collision events (described in detail in Ref. 10). While the time at which cell crossings and carbon-carbon repulsive and attractive interaction events occur can be calculated analytically from the linearity of the center-of-mass motion, the times for the other atom-atom intermolecular interactions must be computed numerically using the grid-search method elaborated in Ref. 10. The use of cell subdivisions, local clocks, and a binary tree to manage the event calendar is a standard practice in this type of simulation and greatly improves simulation's efficiency.[15]

For the purpose of comparison, a rigid molecular model of methane based on continuous interaction potentials was also implemented. In this model, all intermolecular interactions were assumed to be of Lennard-Jones form:

$$V(r_{ij}) = \epsilon_{ij}\left[\left(\frac{R_{\min}^{ij}}{r_{ij}}\right)^{12} - 2\left(\frac{R_{\min}^{ij}}{r_{ij}}\right)^{6}\right], \tag{13}$$

where $R_{\min}^{ij} = \frac{1}{2}(R_{\min}^i + R_{\min}^j)$ and $\epsilon_{ij} = \sqrt{\epsilon_i \epsilon_j}$. Here, ϵ_i and $R_{\min}^i$ represent, respectively, the value and the position of the minimum of the Lennard-Jones potential between atoms of the same kind, i.e., $V(r_{ii})$. The parameters ϵ_i and $R_{\min}^i$ were taken from Ref. 16, where these and other parameters have been computed for atoms in a wide variety of molecules of biological interest and are intended to be used in standard condensed-phase simulations. Standard values were used for all parameters in the continuous-potential system: the C–H bond distance is 1.11 Å, $R_{\min}^{CC} = 3.76$ Å, $R_{\min}^{CH} = 3.07$ Å, $R_{\min}^{HH} = 2.39$ Å, $\epsilon_{CC} = 0.397$ kJ/mol, $\epsilon_{CH} = 0.168$ kJ/mol, and $\epsilon_{HH} = 0.0711$ kJ/mol.

The values of d_{ij} in the DMD model were chosen to be comparable to $R_{\min}^i$, and the DMD results for this methane model presented below were obtained with the following parameter values: $d_{CC} = 3.5$ Å, $d_{HH} = 2.5$ Å, $d_{CH} = 3.1$ Å, $d_{SW} = 5.1$ Å, and $V_{SW} = 1.824$ kJ/mol.

The SMD simulations were carried out using a new rigid-body integration algorithm[9] that makes use of the exact solution of the evolution equations of the attitude matrix.[17] The integration scheme is both symplectic and time reversible, which ensures its stability and lack of systematic energy drift. Unlike other integration schemes, the new method explicitly conserves the total angular momentum vector of the system while generating accurate trajectories. Since the free rotational motion is treated exactly during the torque-free propagation step in a Verlet-like scheme,[12] the integration algorithm typically allows a slightly larger time step to be utilized for a given level of accuracy.[9]

To further enhance the efficiency of the SMD simulations, the forces and torques were calculated using Verlet lists and cell structures.[15] The Lennard-Jones potentials were truncated and smoothly interpolated to zero at a distance of 2.5σ, where $\sigma = 2^{-1/6}R_{\min}$ for each interaction.

All simulations were performed using molecular dynamics simulations with initial configurations drawn from a canonical distribution at a temperature T.[13] To assess the accuracy of the trajectories, the change in energy during the simulated trajectory, $\Delta\mathcal{E} = \mathcal{E}(t) - \mathcal{E}(0)$, can be used. For the DMD simulation, the event-search routine was accurate enough to get $\Delta\mathcal{E} = 0$ for all simulated trajectories. For SMD simulations, the equations of motion of the system are numerically integrated with a small time step to ensure a small value of $\Delta\mathcal{E}$.

B. Low density results

To study a low density methane system, DMD and SMD simulations were performed for the models introduced above. In both cases, a system with 512 molecules was simulated at a temperature $T = 298$ K ($k_B T = 2.478$ kJ/mol) and a density of 3.47×10^{-3} g/cm^3.

In order to give correct time correlation functions, the dynamics calculated in the simulations must take place at constant total energy. To properly generate the correct dynamics and compute time correlation functions, a large num-

Downloaded 14 May 2007 to 142.150.224.6. Redistribution subject to AIP license or copyright, see http://jcp.aip.org/jcp/copyright.jsp

ber of trajectories were generated with no thermostating or other form of energy adjustment from a set of initial conditions drawn from the canonical distribution. Unlike the case of DMD in which the trajectories are exact (up to machine precision), the time step in the SMD simulations must be chosen so that the average fluctuations in the total energy are not larger than some critical value percentage, say, 0.1%, of the average fluctuations in the potential energy. To meet this requirement, a time step of 8 fs was used in the low density SMD simulations.

The average energy in the DMD simulation was found to be 7.36 ± 0.01 kJ/mol. The pressure was calculated using the standard impulsive limit formula[15] and was found to be 5.293 ± 0.007 bars. The corresponding values of the energy and pressure in the SMD simulations were 7.3626 ± 0.0001 kJ/mol and 5.4529 ± 0.0008 bars, respectively.

Although ideally, one would like to simulate a system at standard pressure (1 bar), the pressure in a simulation at constant volume and energy is very sensitive to small changes in the parameters of the interaction potential. This is true for both the DMD and the SMD simulation techniques. For this reason, pressures which do not differ by an order of magnitude (such as those above) may be considered as being in reasonable agreement.

In Fig. 1, the intermolecular carbon-carbon, carbon-hydrogen, and hydrogen-hydrogen radial distribution functions (RDFs) obtained from the DMD simulation are shown as a function of radial distance, and compared to those obtained from the SMD simulation. From the lack of spatial correlation evident in these RDFs, it is clear that the structure of the fluid is that of a gas, which is the expected phase at this density and temperature. Note that the agreement between the carbon-hydrogen and hydrogen-hydrogen RDFs is quite good, while the carbon-carbon RDFs exhibit a clear difference in the shape of the only peak that appears. The difference between the two models in the peak structure for the carbon-carbon RDFs is to be expected since there is no interaction between molecules separated by a distance greater than the square-well parameter (5.1 Å) in the DMD model. In the continuous model, on the other hand, the interaction distance extends up to a cutoff of 2.5σ which corresponds to 8.38, 6.84, and 5.32 Å for the CC, CH, and HH interactions, respectively.

A quantitative comparison of the RDFs can be carried out by calculating the average number q_{AB} of atoms of type B that are close neighbors of an atom of type A, where q_{AB} is given by

$$q_{AB} = 4\pi\rho_B \int_{r_1}^{r_2} r^2 g_{AB}(r) dr, \tag{14}$$

where ρ_B is the number density of type B and $g_{AB}(r)$ is the radial distribution function for the pair AB. With the choice of $r_1=0$ and $r_2=6.7$ Å, one finds that $q_{CC}=0.17$ from the carbon-carbon RDF for both the discontinuous and continuous-potential models, indicating that the average number of near neighbor molecules around a given molecule is essentially the same in the two models at low density. A similar quality of agreement of all q_{AB} is observed for all other pair types, as is evident in Table I.

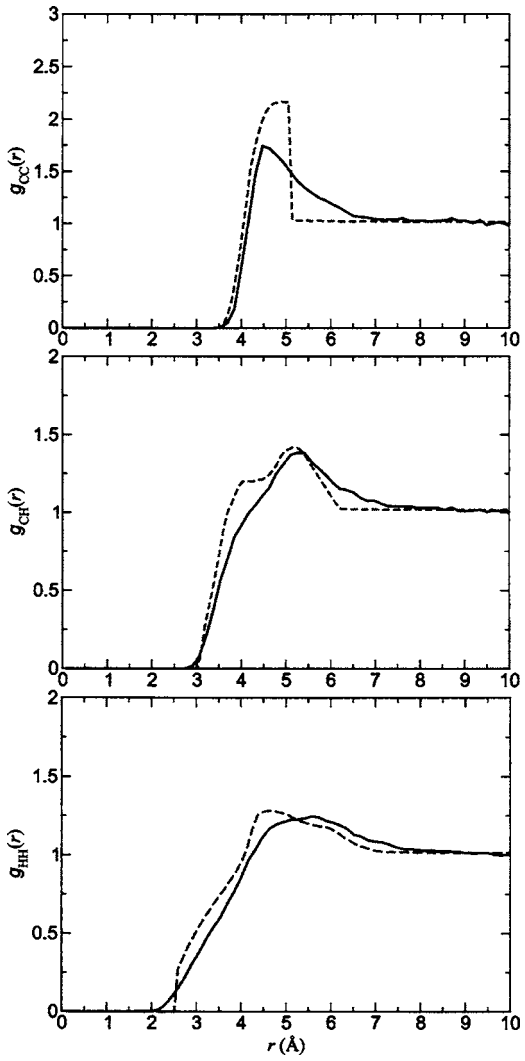

FIG. 1. From top to bottom, carbon-carbon, carbon-hydrogen, and hydrogen-hydrogen RDFs for methane at a gaseous density of 3.47×10^{-3} g/cm^3 and a temperature of 298 K. The continuous lines represent the SMD results and the dashed lines represent the DMD results. The parameters of the model are given in the text.

C. High density results

A more challenging test for the discontinuous model is in the high density and moderately low temperature regime where the system exhibits a liquid behavior and more complex structure. The conditions simulated here correspond to a density of 0.347 g/cm^3 and a temperature of 126.8 K ($k_BT=1.064$ kJ/mol). Under these conditions, the average total

TABLE I. Number of nearby atoms associated with the various peaks of the RDFs for the low density methane fluid presented in Fig. 1. The values are calculated using Eq. (14).

AB	r_1-r_2 range	q_{AB} (DMD)	q_{AB} (MD)
CC	0–6.7 Å	0.171 ± 0.006	0.166 ± 0.012
CH	0–6.7 Å	0.68 ± 0.02	0.66 ± 0.05
HH	0–6.7 Å	0.68 ± 0.03	0.65 ± 0.05

Downloaded 14 May 2007 to 142.150.224.6. Redistribution subject to AIP license or copyright, see http://jcp.aip.org/jcp/copyright.jsp

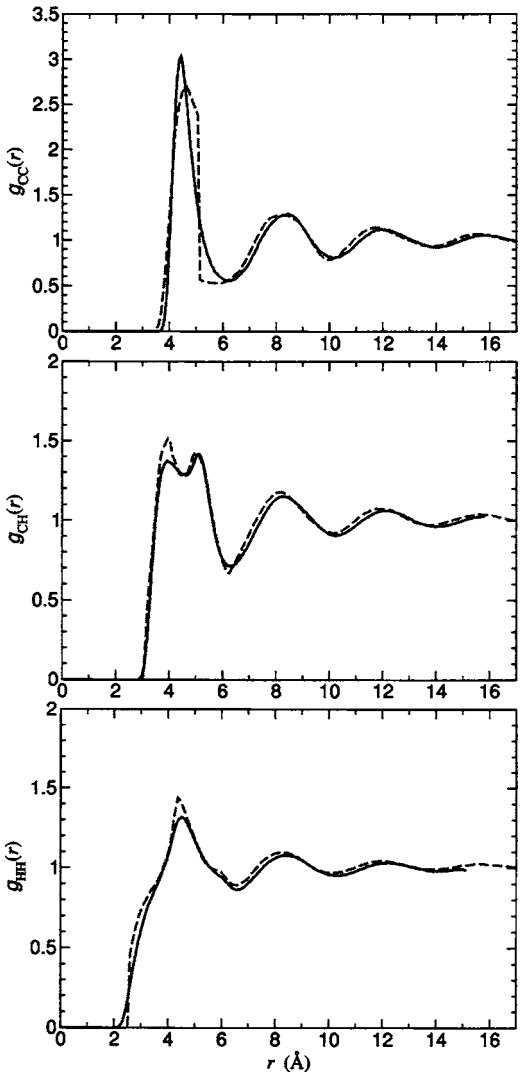

FIG. 2. From top to bottom, carbon-carbon, carbon-hydrogen, and hydrogen-hydrogen RDFs for methane at a liquidlike density of 0.347 g/cm^3 and a temperature of 126.8 K. The continuous lines represent the SMD results and the dashed lines represent the DMD results. Model's parameters are given in the text.

energies in the DMD and continuous-potential model simulations were found to be -3.719 ± 0.005 and -4.613 ± 0.001 kJ/mol, respectively, with corresponding pressures of 774 ± 15 and 850 ± 2 bars (which are in reasonable agreement in the sense explained above).

In Fig. 2, the intermolecular carbon-carbon, carbon-hydrogen, and hydrogen-hydrogen RDFs are plotted versus radial distance. The correlation functions show a highly ordered fluid and are consistent with a liquid phase. Note that most features in the RDFs obtained from the SMD simulations are well reproduced in the DMD simulations.

For a quantitative comparison, we again examine the average number of near neighbors q_{AB}, as defined in Eq. (14). The results are presented in Table II. From the values associated with the first peak in the carbon-carbon RDFs, we see that every molecule is surrounded on average by about 13 other methane molecules in both models. Furthermore, the second peak integrates to about 46, a value that agrees within statistical uncertainties with the value of 45 found

TABLE II. Number of nearby atoms associated with the various peaks of the RDFs for the methane fluid presented in Fig. 2. The values are calculated using Eq. (14).

AB	r_1-r_2 range	q_{AB} (DMD)	q_{AB} (SMD)
CC	0–6.2 Å	12.9±0.3	12.9±0.3
CC	6.2–10.2 Å	45.6±0.9	44.8±0.9
CH	0–6.2 Å	52.6±1.4	51.7±1.3
HH	0–6.6 Å	60.0±2.0	59.6±1.8

with the continuous model. Given that this distance is well beyond the square-well interaction range, the good agreement suggests that excluded volume effects are the predominant factor in the structural packing in this simple liquid system, while details of specific interactions are relatively unimportant.

It is also worth noting that the agreement between the models found in the structural functions at both densities for the same temperature and similar pressure values suggests that they would have a similar phase diagram. An exhaustive analysis of the phase diagram of this model is, however, beyond the scope of this paper.

In addition to the structural properties of the DMD model, event-driven simulations also enable dynamical correlations to be computed in rigid-body systems. In fact, unlike SMD, the DMD approach allows dynamical properties to be calculated from essentially exact (i.e., up to machine precision) trajectories due to the simplicity of the form of the interaction potential. Figure 3 shows the results obtained for the normalized time autocorrelation function of the center-of-mass velocity (VACF) of a given molecule in the fluid, $C(t)=\langle \boldsymbol{V}(0)\cdot\boldsymbol{V}(t)\rangle/\langle \boldsymbol{V}(0)\cdot\boldsymbol{V}(0)\rangle$, for the continuous and discontinuous-potential models under liquid conditions. Considering the fundamental differences in the nature of motion in the two models, the agreement at a qualitative level of $C(t)$ between the two models is somewhat surprising. Nonetheless, it is evident that the short-time behavior, in which the VACF in the DMD model decays more quickly than in the continuous-potential model, and the degree of anticorre-

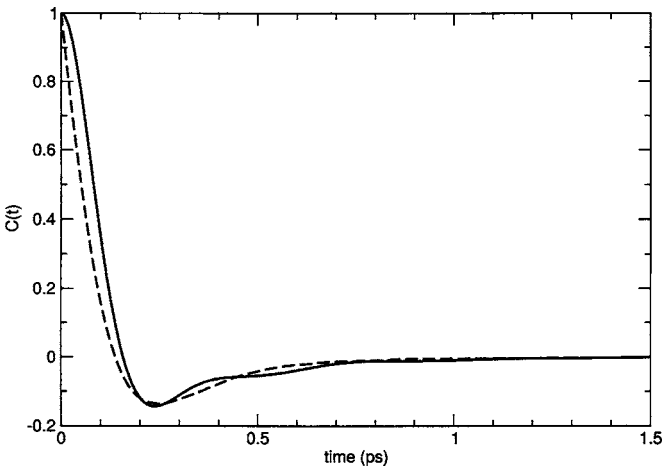

FIG. 3. Velocity time correlation function for the case of liquid methane of Sec. II C. The continuous and dashed lines correspond to the SMD and DMD results, respectively.

Downloaded 14 May 2007 to 142.150.224.6. Redistribution subject to AIP license or copyright, see http://jcp.aip.org/jcp/copyright.jsp

lation in the velocities or "cage" effect at longer time scales differ appreciably. Correspondingly, the values of the self-diffusion coefficient, $D=(k_BT/m)\int_0^\infty C(t)dt$, are found to be $(0.89\pm0.03)\times10^{-5}$ and $(2.64\pm0.06)\times10^{-5}$ cm^2/s for the DMD and SMD simulations, respectively.

D. Efficiency

Given the complexity of constructing an event-driven simulation for rigid systems, it is natural to wonder whether it is worthwhile to carry out such calculations. Such concerns can only be addressed by considering the relative efficiency of event-driven versus standard simulations as a function of the system size and of the physical conditions of the simulation. In order to assess the relative computational efficiency of the DMD simulation, the CPU time needed to simulate 1 ps of real time dynamics was assessed for the DMD and SMD simulations for different system sizes and densities. Of course, such a comparison depends sensitively on a number of factors that have little to do with the methods themselves, such as the choice of programming language, computer architecture, compiler choice, and degree of compiler optimization. In order to minimize such external effects, both the DMD and SMD codes were written in the same high level language (C++), compiled with the same compiler, on the same computer cluster, and with the same nonspecialized level of optimization.

It is also clear that the efficiency of a SMD simulation is largely dependent on the size of the time step chosen to integrate the equations of motion, i.e., the larger the time step the more rapidly the simulation propagates the system. However, a large integration time step leads to numerical instabilities in the MD trajectory, something that can only be tolerated with an extensive use of thermostats. The use of thermostated dynamics has its own limitations since it artificially biases the "true" dynamics and has an influence on the calculation of dynamical properties. Since the effect on the dynamics due to thermostats is generally unknown, no thermostats were used in the SMD simulations after systems were equilibrated. The time step was chosen in our simulations so that no discernible average drift in the total energy was observed over a 10 ps interval, while restricting the fluctuations in the total energy to a thousandth (0.001) of the fluctuations in the potential energy. This procedure resulted in a time step of 8 fs for the low density runs and 3.5 fs for the high density simulations of the continuous-potential system.

The efficiency of the simulations in the discontinuous model depends on the grid time interval used in the root search. In general, one can use the angular velocities of the colliding molecules to extract an average oscillation frequency of the collision indicator function and estimate the appropriate grid time interval for the simulation[18] from this information. In such an approach, the angular velocities, and hence the value of the grid interval, vary with temperature in much the same way that the optimum time step value changes in a continuous MD simulation with temperature. Instead, we have chosen to use k_BT as the energy unit in the simulation so that the average angular velocities in the body frame have the same numerical value regardless of the temperature. This approach has the benefit that the value for the optimal grid time interval is independent of the temperature. With this choice of energy scale, the grid interval was chosen to be 0.2 reduced time units, which corresponds to real time intervals of 12.8 and 19.5 fs for the simulations of gaseous and liquid methane, respectively.

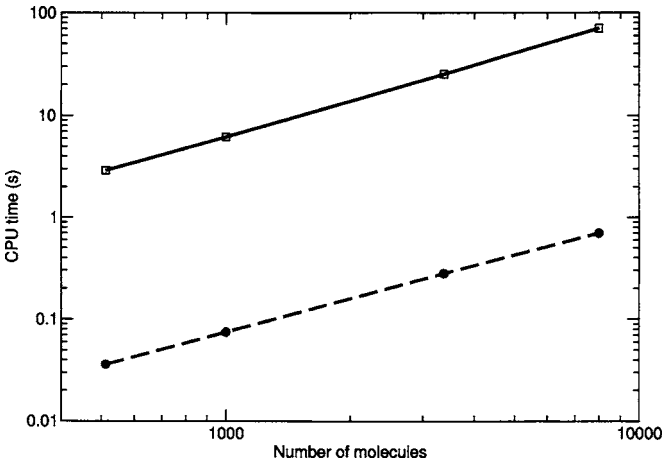

FIG. 4. CPU time per picosecond of real time as a function of the system size for the low density methane case of Sec. II B. The dots correspond to the DMD values whereas the open squares are the values obtained in a continuous MD simulation. The solid and dashed lines join the DMD and MD values and show the expected linear scaling with system size.

Figure 4 shows the CPU time in seconds required by the two methods to simulate 1 ps of real time dynamics for the low density system as a function of the number of molecules. Note that the DMD approach is faster than the SMD simulation by two orders of magnitude for all system sizes. This result is understandable on the basis that the dynamics in a low density system is dominated by free molecular motion over finite time intervals, which, as discussed earlier, can be integrated exactly. This is to be contrasted with the SMD simulation in which an (ideally infinitesimally) small time step must be utilized in order to numerically integrate the dynamics and conserve energy. We also observe in Fig. 4 that both methods scale linearly with system size due to the use of cell lists in the case of the DMD and Verlet lists, cells, and truncated potentials in the case of the SMD system.

Figure 5 shows the CPU time needed by the DMD and SMD methods to carry out 1 ps of real time dynamics for the denser system at 0.347 g/cm^3. The insert shows the ratio of the CPU time per picosecond of the SMD to DMD simulations and indicates that, even at this density, the DMD method is more than three times more efficient than the highly optimized SMD method.

One clear disadvantage of performing DMD simulations on rigid bodies as opposed to simple hard spheres is the necessity to find collision times using numerical root-search methods. The evaluation of distances between possibly interacting atoms is computationally costly and is often the most demanding task in a DMD simulation of rigid systems. To reduce the computational work of finding collision times, it is convenient to truncate the numerical search of collisions that extend beyond a certain maximum time interval, which will be called the *search interval*, since events far in the

Downloaded 14 May 2007 to 142.150.224.6. Redistribution subject to AIP license or copyright, see http://jcp.aip.org/jcp/copyright.jsp

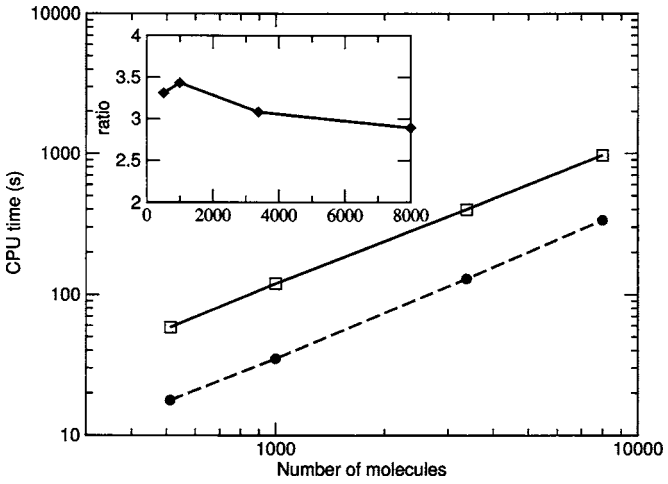

FIG. 5. CPU time per picosecond of real time as a function of the system size for the high density methane case of Sec. II C. The dots correspond to the DMD results and the open squares correspond to the continuous MD simulation. The insert shows the ratio of the SMD to DMD CPU time for simulating 1 ps as a function of system size.

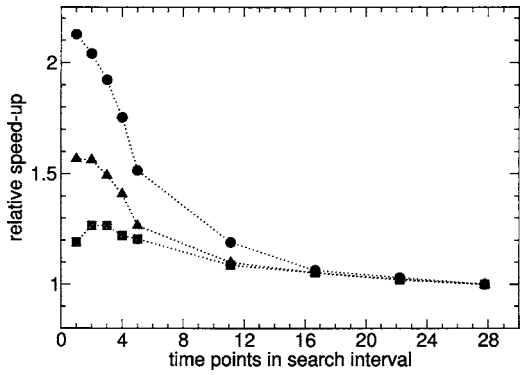

FIG. 6. The relative speedup due to the use of virtual collisions as measured by the ratio of the CPU time for simulating liquid methane for 1 ps without and with virtual collisions as a function of the number of time points in the search interval. The circles, triangles, and squares correspond to the system with 1000, 3375, and 8000 methane molecules, respectively.

future are not likely to be executed. To implement a truncation scheme, collisions found in the search interval are scheduled as such, while collisions which may still potentially occur, but were not found within the search interval, are scheduled as a *virtual collision* (see Ref. 10), much as if it were a possible future collision. If the virtual collision, scheduled between atoms i and j, is relatively far in the future, it is quite likely that these atoms will interact with other atoms before their virtual-collision event is processed. If this is not the case and indeed the virtual collision must be executed, the root search is continued from where it was previously stopped. In this way, the numerical effort is primarily focused on the most likely events (i.e., the ones happening within the search interval) and the number of grid evaluations in which the Cartesian positions and the distances between all atoms in the pair of molecules are calculated is diminished. Even though the truncation of the numerical search for collision events reduces the computational load of this type of event, the introduction of new events increases the size and complexity of the binary tree used to manage events. As a result, the scheduling of new events, which typically scales as $N \log N$, where N is the number of events in the tree, becomes more demanding. Since the computational effort associated with the data management increases while the effort of finding collisions decreases, the optimal size of the time interval for the virtual collisions is a function of the size of the tree, and hence the overall size of the system. If the search interval is very large, very few virtual collisions are scheduled and the efficiency of the simulation converges to that of a simulation that does not include virtual-collision events.

Figure 6 shows the relative gain in efficiency due to the use of virtual-collision events for the systems consisting of 1000, 3375, and 8000 molecules as a function of the maximum number of evaluations of the collision function in the search interval. Clearly, the use of virtual collisions increases as this ratio is decreased. For the system with 1000 molecules, an intensive use of virtual collisions (i.e., one or two grid evaluations) doubles the computational efficiency with respect to a simulation not utilizing these types of events. Smaller systems (not shown) exhibit the same trend and have similar relative efficiencies. For a very large system, however, the gain in efficiency is smaller due to the fact that a large binary tree slows down the processing of events. Indeed, for the system with 8000 molecules, it is more efficient to limit the number of virtual collisions scheduled by extending the search up to two or three grid evaluations instead of performing a single grid evaluation per root search. The effect of the increased load in data management can be clearly seen as the system size increases. Nonetheless, the scheduling of virtual collisions leads to significant improvements in simulation efficiency for all system sizes examined where the numerical search for collision times, as opposed to data management, represents the bulk of the computational work in the simulation.

III. BENZENE

A. Molecular model

The methane system considered in the previous section has particularly simple rotational dynamics due to the high degree of symmetry of the methane molecule. However, the formalism established in Ref. 10 allows simulations of rigid molecules with arbitrary mass distribution to be performed. A simple example of slightly more complicated rotational dynamics is that observed in symmetric top molecules, such as benzene, in which two of the principal moments are equal and the third is distinct.

For a system of rigid benzene molecules, there are a total of 13 relevant sites in every molecule; the center of mass, six carbon sites, and six proton sites, where all atoms lie in a single plane with the carbon sites forming a closed ring. However, using a *united-atom* approach, in which every carbon-hydrogen pair is represented as a unique site, the number of relevant sites in every molecule is reduced to 7. If the radial distance from the center of mass to each united "carbon" atom in the plane of the molecule (taken to be the XY plane) is d and the mass of the united atoms is set to $m_{\mathrm{CH}}=13m_p$, then one finds that the principal moments of

Downloaded 14 May 2007 to 142.150.224.6. Redistribution subject to AIP license or copyright, see http://jcp.aip.org/jcp/copyright.jsp

inertia are $I_1=I_2=3m_{CH}d^2=39m_pd^2$ and $I_3=2I_1$.

Typically, the intermolecular interactions between the united atoms in benzene are assumed to be of Lennard-Jones form, leading to an interaction energy that depends strongly on the relative orientations of the interacting molecules. One of the simplest possible discontinuous-potential models possessing attractive but directional interactions consists of a combination of a spherically symmetric attractive square well about each center of mass combined with purely repulsive interactions between united carbon atoms. We therefore consider a united-atom model of benzene in which the center-of-mass site, or site X, is defined to have a repulsive hard-wall interaction with any other center-of-mass site, at the interaction distance d_{xx} while the united carbon sites repel one another at distance d_{CC}. The attractive interaction potential between the centers of mass of two molecules is defined as

$$V_{xx}^{\text{attr}}(r_{xx}^{ab})=\begin{cases}-V_{SW1} & \text{if } r_{xx}^{ab}\leqslant d_{SW1}\\ -V_{SW2} & \text{if } d_{SW1}<r_{xx}^{ab}\leqslant d_{SW2}\\ 0 & \text{if } r_{xx}^{ab}>d_{SW2},\end{cases} \tag{15}$$

where r_{xx}^{ab} is the distance between the center of mass of any two molecules a and b. This potential contains two attractive square-well regions and four parameters: two square-well distances d_{SW1} and d_{SW2}, and two square-well depths V_{SW1} and V_{SW2}.

A DMD simulation with this model can be implemented in the same way as for the methane model in Sec. II, with a slightly more complex propagation matrix $\mathbf{P}(t)$ [see Eq. (4)]. For the symmetric top system, $\mathbf{P}(t)$ can be written as the product of two rotation matrices,[10]

$$\mathbf{P}(t)=\mathbf{U}(-\omega_p t\hat{z})\mathbf{U}\left(-\frac{\tilde{\boldsymbol{L}}_0}{I_1}t\right), \tag{16}$$

where $\omega_p=(1-I_3/I_1)\tilde{\omega}_z(0)$ is called the precession frequency, and $\tilde{\boldsymbol{L}}_0=\tilde{\mathbf{I}}\tilde{\boldsymbol{\omega}}(0)$ is the initial angular momentum vector in the body frame. Unlike the case of the spherical rotor, the x and y components of the angular velocity in the body frame are time dependent, and the moment-of-inertia tensor in the laboratory frame is no longer constant and diagonal.

For the purposes of comparison, a continuous-potential united-atom model of benzene was employed, in which the united atoms interact via intermolecular Lennard-Jones interactions, as defined in Eq. (13). Note that this model does not possess any explicit interactions between centers of mass and that the site-site interactions lead to an effective orientational dependence in the interaction between molecules.

B. Simulation details

Simulations were performed for both models in a box with 512 molecules at a density of 0.870 g/cm^3 with initial conditions drawn from a canonical ensemble at a temperature of 298 K ($k_BT=2.478$ kJ/mol). The distance d between carbon sites (or between the center of mass and every carbon site) was set to 1.48 Å in both models of rigid benzene.

The parameters in the DMD model used to obtain the results presented below are $d_{CC}=3.25$ Å, $d_{11}=2.0$ Å, $d_{SW1}=6.8$ Å, $d_{SW2}=12.8$ Å, $V_{SW1}=1.982$ kJ/mol, and $V_{SW2}=0.446$ kJ/mol. The numerical search for collision events was carried out using a time grid of 19 fs and with only one grid point evaluation in the search interval (i.e., extensive use of virtual collisions).

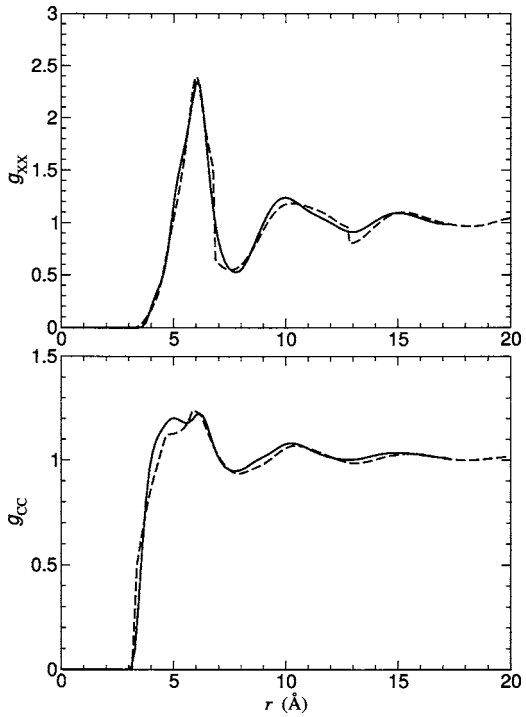

FIG. 7. From top to bottom, center-of-mass–center-of-mass (xx) and carbon-carbon RDFs for liquid benzene. The continuous lines represent the results for SMD simulation and the dashed lines represent those for the DMD model (see Sec. III B for details).

The Lennard-Jones parameters used for united-atom interactions in the continuous model simulations are $\epsilon=0.457$ kJ/mol and $R_{min}=3.695$ Å. As in the case of the simulations of the methane system, the Lennard-Jones interactions were truncated and smoothly interpolated to zero at a distance of $2.5\sigma=9.25$ Å. The SMD simulations were carried out using the same rigid-body integration scheme as for the methane system except that the exact free-flight motion of a symmetric top was used rather than that of a spherical rotor. A time step of 5 fs was used in the numerical integration of the equations of motion. With these parameters, the DMD method was once again roughly three times more efficient computationally (measured as the CPU time needed for the simulation of 1 ps of real time dynamics) than the SMD simulation.

C. Static properties

The canonical average intermolecular energy values obtained for the DMD and the SMD simulations were -23.558 ± 0.005 and -25.4 ± 0.1 kJ/mol, respectively. The pressure values were 930 ± 25 and 360 ± 60 bars for the step potential model and the MD simulation, respectively.

Figure 7 shows the center-of-mass–center-of-mass and carbon-carbon radial distribution functions obtained for the discontinuous and continuous models of liquid benzene. The results agree with one another and with previous molecular

Downloaded 14 May 2007 to 142.150.224.6. Redistribution subject to AIP license or copyright, see http://jcp.aip.org/jcp/copyright.jsp

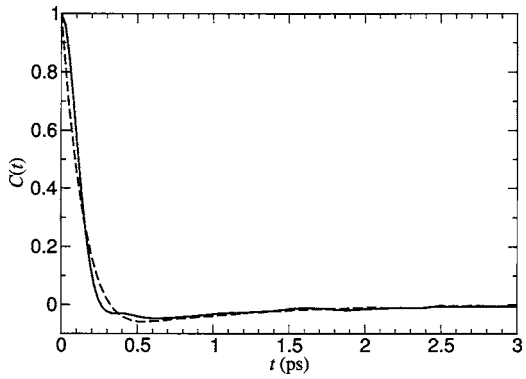

FIG. 8. Normalized velocity time autocorrelation function for liquid benzene. The continuous line corresponds to the result of SMD simulations of the Lennard-Jones continuous potential system and the dashed line corresponds to the results from the DMD simulation.

dynamics studies[19] of liquid benzene at similar densities and temperatures. It is clear that the discontinuous model reproduces most of the structural details found with the continuous model in both radial distribution functions. In Fig. 7, the DMD simulation results for the center-of-mass radial distribution function show two sharp decreases at distances of about 6.8 and 13.8 Å, which coincide naturally with the values of the square-well attractive potential distances chosen for the model. Indeed, these distances were chosen such that the discontinuous model can match the continuous radial distribution functions.

D. Dynamical properties

The normalized center-of-mass velocity time autocorrelation functions obtained from the DMD and SMD simulations are shown in Fig. 8. In spite of the differences between the models, the agreement between the correlation functions is very good. The values of the diffusion coefficients, obtained from integrating the functions in this figure, are $(1.42\pm0.04)\times10^{-5}$ and $(1.62\pm0.04)\times10^{-5}$ cm^2/s for the DMD and SMD simulations, respectively. The values agree well, although both are smaller than the experimental value of 2.27×10^{-5} cm^2/s (Ref. 20) reported at this temperature.

The rotational motion in liquid benzene is more complex than the motion in liquid methane, and in other spherical rotor systems, due to the asymmetry of the benzene molecule. The asymmetry leads to nontrivial orientational components of the static structure in which the planes of nearby benzene molecules tend to be orthogonal to one another. The asymmetry also leads to interesting correlations in rotational motion that can be examined by looking at normalized autocorrelation functions $C_{\omega_k}(t)$ of components of the angular velocity in the body frame,

$$C_{\omega_k}(t) = \langle \tilde{\omega}_k(0)\tilde{\omega}_k(t)\rangle / \langle \tilde{\omega}_k^2(0)\rangle, \tag{17}$$

where the $\tilde{\omega}_k$ are the $k=x,y,z$ components of the angular velocity vector in the body frame. In Fig. 9, the time autocorrelation functions of the x and z components of the angular velocity vector in the body frame are plotted versus time, where x and y are the principal axes in the plane of the molecule and z is the principal axis (C_6 axis) orthogonal to the plane of the molecule. Note that, due to symmetry, $C_{\omega_x}(t)=C_{\omega_y}(t)$.

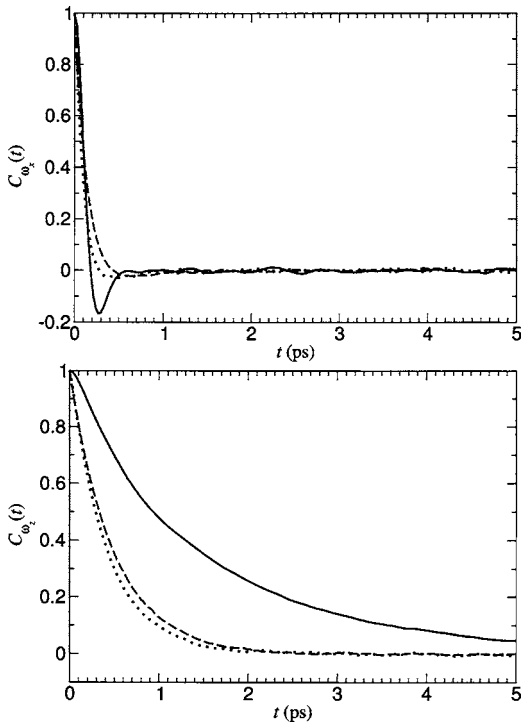

FIG. 9. Time correlation functions of the x and z components of the angular velocity vector in liquid benzene. The continuous line corresponds to the Lennard-Jones potential and the dashed line corresponds to the DMD result. The dotted lines are the results obtained with SMD using the hyperbolic tangent potential defined by Eq. (18).

As can be seen in Fig. 9, the x component of the angular velocity time correlation function from the SMD simulations exhibits a well defined minimum that is not reproduced in the DMD model. Angular correlations of these components are short lived in the dense system, with a lifetime of less than a picosecond, due to the strong confining effect of molecular cages in the liquid. The minimum in $C_{\omega_x}(t)$ calculated in the continuous-potential model reflects an anticorrelation in the angular velocities due to molecules rebounding off of nearest neighbors and is reminiscent of anticorrelations observed in velocity autocorrelation functions. Interestingly, this phenomenon is not observed in the DMD simulation.

In contrast, the autocorrelation function of the z component of the angular velocity has a much longer lifetime in both models, although $C_{\omega_z}(t)$ decays much too quickly in the DMD simulation. The longer lifetime arises due to the relatively free motion of rotations about the z axis of a molecule, corresponding to a planar spinning motion.

In order to understand the origin of some of the deficiencies of the discontinuous model, it is instructive to examine the interaction energy between two benzene molecules, lying in the same plane, as one molecule is rotated relative to the other around the z axis for both models. This interaction energy for the continuous-potential model is plotted in Fig. 10. In the discontinuous model, the rotational motion is completely free unless the centers of mass of the molecules are close enough ($r_{xx}<6.25$ Å) so that a hard-core collision takes place. When the hard-core collision occurs, the z com-

Downloaded 14 May 2007 to 142.150.224.6. Redistribution subject to AIP license or copyright, see http://jcp.aip.org/jcp/copyright.jsp

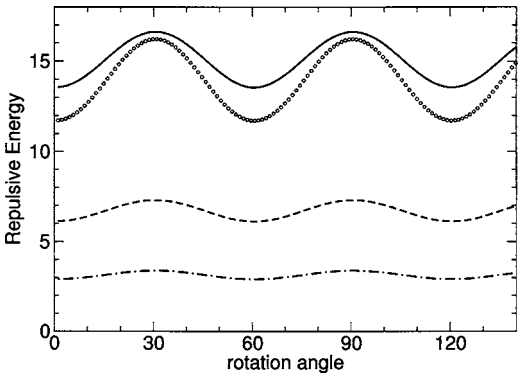

FIG. 10. Repulsive potential energy (in units of k_BT) for the Lennard-Jones system between two benzene molecules as a function of their relative orientation measured by the rotation angle (in degrees) around the z axis of one of the molecules. The continuous, dashed, and dot-dashed lines correspond to coplanar benzene molecules at center-of-mass distances r_{xx} of 6.0, 6.25, and 6.4 Å, respectively. The circles correspond to molecules in orthogonal planes with r_{xx}=6.0 Å.

ponent of the angular velocity in the body frame changes direction and the rotation effectively reverses direction. In contrast, the repulsive energy in the continuous model increases up to a maximum where the distance between united-carbon atoms on the two molecules is minimized. The repulsive energy drops as the molecule rotates past this point, so that there is a "hindered" rotational interaction for the rotation of one molecule past another. Such oscillatory interactions, clearly absent in the DMD model, are responsible for the qualitative differences observed in Fig. 9. An interaction analogous to the one shown in Fig. 10 can be included in the DMD model by adding finite repulsive shoulder interactions between united carbon atom sites.

Alternatively, the role of the hindered rotational interactions on the angular correlations can be isolated by systematic modifications of the continuous-interaction potential to approach the discontinuous limit and, therefore, the DMD model. For example, instead of using a Lennard-Jones interaction, repulsions between united carbon atoms can be modeled with a potential of the form

$$V_{ij}^{\mathrm{rep}}(r_{ij}^{ab}) = \alpha_1 \tanh[\alpha_2(d_{ij} - r_{ij}^{ab})]. \tag{18}$$

Parameters α_1 and α_2 can be independently assigned to control the height and the width of the repulsive potential, respectively. The value of α_1 can be set large enough that the probability of any molecule going through the barrier is virtually zero. The hard-wall limit in which the interaction range approaches zero and interactions become instantaneous is formally obtained in the limit of infinite α_2. Of course, such a potential cannot be integrated numerically, and comparisons of dynamics using numerical-integration schemes and dynamics in the impulsive limit must use a large, but finite value of α_2.

As an illustration of how the limit of an infinitely steep potential is approached, consider the trajectories of two benzene molecules before and after their mutual interaction through the potential defined by Eq. (18). In Fig. 11, the dynamical evolution of separate components of the linear and angular velocity vectors of one of the molecules involved in the collision is shown as a function of time for the

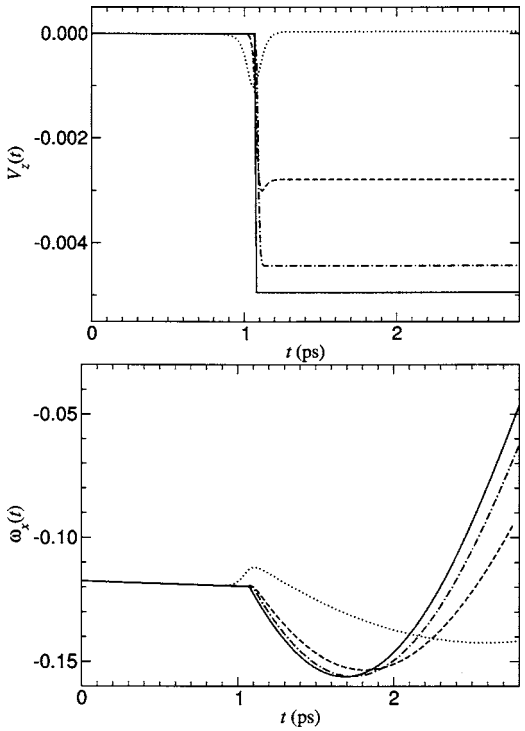

FIG. 11. Time evolution of the z component of the velocity vector (top panel) and the x component of the angular velocity vector (bottom panel) of a benzene molecule involved in a collision with another benzene molecule. The solid lines correspond to the DMD simulation. The dot, dashed, and dot-dashed lines correspond to the model interactions given by Eq. (18) with α_2 values of 5, 10, and 20, respectively.

DMD model. The trajectories in the impulsive limit are also included in this figure for comparison. Since the center-of-mass velocity vector, its components, and the z component of the angular velocity vector are constants of the motion, their behavior is analogous to the one shown in the top panel of Fig. 11. It is clear that the interaction time goes to zero and the final v_z value approaches the DMD result as the value of α_2 increases. The x and y components of the angular velocity vector, on the other hand, follow an oscillatory dynamical pattern and their time evolution after the interaction can be quite different than that observed in the impulsive limit, as can be seen in the bottom panel of this figure. Once again, one observes that the dynamics generated by the continuous potential approaches the DMD as the value of α_2 increases.

The time correlation results obtained with SMD simulations of a system composed of 512 benzene molecules interacting via Eq. (18), at the same density and temperature as above, are also shown in Fig. 9. These results are obtained with the values α_1=40 and α_2=20 for the carbon-carbon repulsion. Not surprisingly, the new time correlation functions agree much better with results obtained with the DMD model than those of the Lennard-Jones model. This agreement confirms that the discrepancies observed in the angular velocity correlation functions in the discontinuous and continuous models are a consequence of the overly simplistic interaction potential between united carbon sites.

In addition to correlation functions of the angular velocities, one can also examine how long individual benzene molecules retain their orientation in a dense liquid. One common

Downloaded 14 May 2007 to 142.150.224.6. Redistribution subject to AIP license or copyright, see http://jcp.aip.org/jcp/copyright.jsp

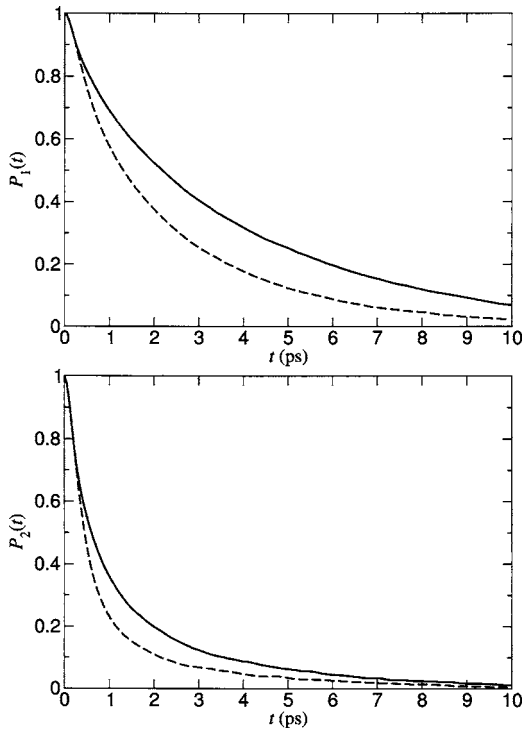

FIG. 12. Orientational time correlation functions $P_1(t)$ and $P_2(t)$ in liquid benzene. The continuous line corresponds to the Lennard-Jones potential and the dashed line corresponds to the DMD result.

measure of orientational correlation involves computing ensemble averages of low order Legendre polynomials of the cosine of the angle between an orientational vector of a molecule, such as the C_6 axis (or z axis), at two times. In Fig. 12, the $P_1(t)$ and $P_2(t)$ orientational time correlation functions defined by

$$P_1(t) = \langle \hat{z}(0) \cdot \hat{z}(t) \rangle \tag{19}$$

and

$$P_2(t) = \left\langle \tfrac{1}{2}\{3[\hat{z}(0) \cdot \hat{z}(t)]^2 - 1\} \right\rangle \tag{20}$$

for the DMD and Lennard-Jones models are shown. The overall shape of these functions is in agreement with previous molecular dynamics simulations of liquid benzene.[21] Although there is qualitative agreement in orientational correlations in the continuous and discontinuous models, again it is evident that orientational correlations typically decay more quickly in the discontinuous model than in the continuous model. It is likely that the longer-lived orientational correlations in the continuous case arise due to the hindered rotational interactions that are poorly modeled in the simple discontinuous system.

IV. CONCLUSIONS

In this paper DMD simulations of two rigid molecular systems, which differ in the symmetry of their mass distribution, were presented. The simulation methodology utilized is based on exact solutions of the free motion of rigid bodies in combination with collision rules derived from conservation laws.

In Sec. II, a discontinuous model of rigid methane was constructed in which methane molecules attract one another via a center-of-mass square-well potential, while the constituent atoms of different molecules repel each other through hard-core repulsions. DMD simulations of the spherical rotor system were carried out in low and high density regimes, and excellent agreement with standard molecular dynamics simulations was observed for all structural quantities. It was furthermore found that dynamical quantities, such as the self-diffusion coefficient, also agree well with those of standard MD simulations.

In addition, the efficiency of DMD simulations relative to continuous-potential simulation methods of the rigid methane system was examined in order to assess the role of certain parameters such as the grid-search size and the truncation interval for the root search in the DMD simulations. It was found that the DMD simulations were between 3 and 100 times more efficient than SMD simulations at densities of 0.347 and 3.47×10^{-3} g/cm^3, respectively. Furthermore, it was found that it is generally most efficient to schedule virtual-collision events as frequently as possible for small systems and slightly less frequently for larger systems. The use of virtual-collision events typically leads to improvements in efficiency of 25% for large systems and up to 110% for small systems.

A united-atom model with discontinuous potentials for rigid benzene was presented in which benzene molecules attract one another via center-of-mass interactions, while united carbon atoms repel one another via hard-core interactions. DMD simulations of the rigid benzene system at a liquid density were carried out using the simulation methodology appropriate for a symmetric top rigid body. To the best of our knowledge, this is the first event-driven simulation of a nonspherical rigid body, other than a linear dumbbell, where the dynamics and collision rules are properly taken into account without approximation of the dynamics or collision rules. Static and dynamical quantities from the DMD simulation were compared with those obtained from a continuous-potential benzene model, in which the united carbon atoms interact via a standard Lennard-Jones potential and found to be in good agreement. The quantitative discrepancies in dynamical correlations of angular velocities and orientational directors between the models are readily explained in terms of the crude level of description in the discontinuous model of the hindered rotational motion of one benzene molecule near another. Nonetheless, one can argue that the relevant physics is already present in the crude description of the interactions in the DMD model, such as long-lived orientational correlations and correlation times of ω_z which are significantly larger than those of ω_x and ω_y. If one is interested in more detailed features of the dynamics, it is always possible to add more discontinuities in the interactions, at the expense of computational efficiency.

The major purpose of this work is to establish that event-driven simulations of rigid molecular systems can be carried out with impressive gains in efficiency over standard molecular dynamics methods. Of course, the magnitude of the gain in relative efficiency depends on a number of factors, such as the level of detail in constructing a discontinuous-

Downloaded 14 May 2007 to 142.150.224.6. Redistribution subject to AIP license or copyright, see http://jcp.aip.org/jcp/copyright.jsp

potential model of the system, the system size, and physical parameters such as the density. Nonetheless, our results indicate that the gain in efficiency through the use of crude discontinuous-potential models of condensed-phase systems may allow larger systems or longer time scales to be investigated than those currently accessible with standard simulation methods.

ACKNOWLEDGMENTS

One of the authors (S.B.O.) gratefully acknowledges Evan O'Connor for useful discussions. This work was supported by grants from the Natural Sciences and Engineering Research Council of Canada (NSERC).

[1] B. J. Alder and T. E. J. Wainwright, J. Chem. Phys. **31**, 459 (1959).
[2] D. C. Rapaport, J. Chem. Phys. **71**, 3299 (1979).
[3] A. Bellemans, J. Orban, and D. VanBelle, Mol. Phys. **39**, 781 (1980).
[4] G. A. Chapela, S. E. Martínez-Casas, and J. Alejandre, Mol. Phys. **53**, 139 (1984).
[5] G. A. Chapela, H. T. Davis, and L. E. Sciven, Chem. Phys. **129**, 201 (1989).
[6] Y. Zhou and M. Karplus, J. Mol. Biol. **293**, 917 (1999).
[7] F. Ding, J. M. Borreguero, S. V. Buldyrey, H. E. Stanley, and N. V. Dokholyan, Proteins: Struct., Funct., Genet. **53**, 220 (2003).
[8] H. D. Nguyen and C. K. Hall, J. Am. Chem. Soc. **128**, 1890 (2006).
[9] R. van Zon and J. Schofield, e-print cond-mat/0612404.
[10] L. Hernández de la Peña, R. van Zon, J. Schofield, and S. B. Opps, J. Chem. Phys. **126**, 074105 (2007), preceding paper.
[11] This exactness applies to the free-flight portions of the motion (due to the rigidity of the molecules) and the collision rules. The time of a collision event cannot be expressed in an exact closed form in general, yet it can be determined to arbitrary precision (in practice machine precision) using any of a number of numerical procedures.
[12] A. Dullweber, B. Leimkuhler, and R. McLachlan, J. Chem. Phys. **107**, 5840 (1997).
[13] Such initial conditions can be found using a hybrid Monte Carlo method [see, e.g., S. Duane, A. D. Kennedy, B. J. Pendleton, and D. Roweth, Phys. Lett. B **195**, 216 (1987)], which can be realized within the context of simulating rigid bodies, since the dynamics in these simulations is *time reversible* and *area preserving*, being derived from a Hamiltonian.
[14] W. H. Press, S. A. Teukolsky, W. T. Vetterling, and B. P. Flannery, *Numerical Recipes in Fortran; The Art of Scientific Computing*, 2nd ed. (Cambridge University Press, Cambridge, 1992).
[15] D. C. Rapaport, *The Art of Molecular Dynamics Simulation* (Cambridge University Press, Cambridge, 2004).
[16] A. D. MacKerell, Jr., D. Bashford, M. Bellott *et al.*, J. Phys. Chem. B **102**, 3586 (1998).
[17] R. van Zon and J. Schofield, J. Comput. Phys. (in press).
[18] C. De Michele, S. Gabrielli, P. Tartaglia, and F. Sciortino, J. Phys. Chem. B **110**, 8064 (2006).
[19] N. Zacharopoulos, N. Vergadou, and D. N. Theodorou, J. Chem. Phys. **122**, 244111 (2005).
[20] D. R. Falcone, D. C. Douglass, and D. W. McCall, J. Ceram. Soc. Jpn. **71**, 2754 (1967).
[21] I. Cacelli, G. Cinacchi, G. Prampolini, and A. Tani, J. Am. Chem. Soc. **126**, 14278 (2004).

Downloaded 14 May 2007 to 142.150.224.6. Redistribution subject to AIP license or copyright, see http://jcp.aip.org/jcp/copyright.jsp